HAL open science

Anisotropy of the triboelectric effects in polymeric slabs

Horia-Nicolai Teodorescu, Yopa Prawatya, Thami Zeghloul, Lucian Dascalescu

To cite this version:

Horia-Nicolai Teodorescu, Yopa Prawatya, Thami Zeghloul, Lucian Dascalescu. Anisotropy of the triboelectric effects in polymeric slabs. Tribology International, 2019, 136, pp.496-507. 10.1016/j.triboint.2019.04.014 . hal-02326548

HAL Id: hal-02326548

https://hal.science/hal-02326548v1

Submitted on 22 Oct 2021

HAL is a multi-disciplinary open access archive for the deposit and dissemination of scientific research documents, whether they are published or not. The documents may come from teaching and research institutions in France or abroad, or from public or private research centers.

L'archive ouverte pluridisciplinaire **HAL**, est destinée au dépôt et à la diffusion de documents scientifiques de niveau recherche, publiés ou non, émanant des établissements d'enseignement et de recherche français ou étrangers, des laboratoires publics ou privés.

Distributed under a Creative Commons Attribution - NonCommercial 4.0 International License

Version of Record: https://www.sciencedirect.com/science/article/pii/S0301679X19302087
Manuscript_61f6ac44b23850b9b41a6efd5f07d0a6

Anisotropy of the triboelectric effects in polymeric slabs

Horia-Nicolai Teodorescu[1,2], Yopa Prawatya[3], Thami Zeghloul[3], Lucian Dascalescu[3]

[1,2] *Romanian Academy – Iasi Branch, Bd Carol I nr. 8, and*

"G. Asachi" Technical University, 67, Bd. D. Mangeron, 700050 Iasi, Romania

[3]*PPRIME Institute, CNRS – University of Poitiers – ENSMA, 4 av. Varsovie, 16021 Angoulême, France*

Highlights

* Triboelectric charging of polymeric slabs may be direction-dependent
* Tribocharging anisotropy is partly due to direction-dependent superficial roughness
* Surface electric potential maps depend significantly on the sliding direction
* Non-uniformity of surface electric potential produces large local electric fields
* Average surface electric potential is higher along the direction of higher roughness

Abstract

The paper contributes to the understanding of triboelectric charging mechanisms. It brings evidence of the fact that in polymer slabs this effect may present significant direction dependence (anisotropy) related to the initial superficial roughness. The study was carried out on Polyvinyl Chloride (PVC) slabs in frictional sliding conformal contact with Acrylonitrile Butadiene Styrene (ABS) slices. It showed that the anisotropy of tribocharging is correlated to that of initial surface patterns (texturing) specific to polymer manufacturing process. The effect is preserved for small numbers of repeated movements even when moderate wearing occurs. Conclusions are derived for improving triboelectric energy harvesters, sensors, and other applications.

Keywords: triboelectrification, direction-dependence, sliding, polymers, potential profile

1. Introduction

The study of triboelectric charge generation has seen a revived interest during the last 10 years because of its numerous potential applications. Thus, friction reduction in various types of mechanisms can be achieved by an external electric field orthogonal to the lubricated contact [1] – [3]. Same effects can be obtained when the electric field is generated by the electric charges separated by the triboelectric effect on polymers surfaces in sliding frictional

© 2019 published by Elsevier. This manuscript is made available under the CC BY NC user license
https://creativecommons.org/licenses/by-nc/4.0/

conformal contact [4], [5]. Several tribocharging devices have been developed [6] – [9], for being used in conjunction with free-fall or roll-type electrostatic separation [10], [11]. The tribocharging effect is more and more widely used for energy harvesting [12] – [20], i.e., the conversion of the frictional motion between dissimilar bodies into electric power. Such triboelectric generators can be employed as sensors [21] – [23], for a number of applications, including pressure measurement [24], as well as texture and sliding motion sensation [25].

The anisotropy of tribology effects has been put into evidence in many papers [26] – [30]. The theoretical and experimental studies reveal the effects of surface texturing on the friction forces in both lubricated and unlubricated contacts [31]-[34]. It can be assumed that the triboelectric effect is also direction-dependent.

However, the anisotropy of triboelectric charging has not been addressed yet. There are several applicative and theoretical reasons to investigate the direction dependence of the triboelectric effect. In domains where the triboelectric charging is undesired, such as in mechanisms with plastic parts, understanding the role of anisotropy may help in reducing the electrostatic hazard related to this phenomenon. In applications where triboelectric charging is useful, such as energy harvesters, optimization of the outcome may be possible by taking advantage of the anisotropy of the process as long as the wearing of the surfaces is low.

The triboelectric effect [35], [36] consists in a set of phenomena involving physical (mechanical, thermal, electrical) and chemical processes [37], as well as the geometrical and statistical properties of the surface pattern [36]. In particular, triboelectric charging in polymers is a complex process involving many inter-related phenomena, such as chemical bonding and bond rupture, energy levels in macromolecules, formation of radicals, charge mobility, thermal dissipation, surface electric charge distribution, electromagnetic radiation generation, and possibly others [38] – [41]. The charge generation induced by friction and deformation (elongation, compression), and fracture involves molecular and macroscopic processes. All friction processes induce microscopic deformations and fracture (the last one best known as abrasion and ‘wearing’), as well as thermal effects. Hereafter, these processes are reviewed in relation with their potential dependence on the direction of movement of the contact surfaces.

It is believed that a common mechanism that produces charging of polymer samples during friction with wearing is bond cleavage, also named bond scission. The proof of this effect was given among others by Dickinson et al. [42] – [45], who found evidence that carbon oxide molecules are released during bond cleavage in polycarbonate mechanically loaded up to failure at room temperature. This mechanism of charge generation is prone to

show directional effects in polymeric materials with oriented molecular chains (structural anisotropy). Therefore, this mechanism is likely to be involved in the triboelectric charge generation process described in the present paper and which was related to the frictional contact between polymer slabs characterized by anisotropic initial surface patterns.

The charge generation can be different in various materials, depending on the molecular orbital energy and its distance to the Fermi level, with nonlinear effects occurring when the two energy levels are close [46]; higher friction coefficient in a specified direction helps attaining the threshold of charge generation at lower friction forces and thus induce a directional-dependent effect of charging.

In an early paper, Henry [47] has shown that there are essentially two different effects that lead to tribocharging: the surface contact charging, not needing any friction and essentially anisotropic, and the friction-induced charging, that may occur for same type of materials under friction. The second process, Henry suggested, is potentiated by local differences between the properties of the two surfaces and by thermal gradients induced by friction [47]. Dickinson and Jensen [43] argue that the heating of the insulating polymers due to friction also plays an important part in the charge generation. The heat stimulates free charge generation. Higher friction coefficient in a specified direction would increase the heat dissipation and thus enhance charge production. However, temperature exponentially increases the conductivity of the dielectrics and may lead to faster decay of the charge.

There are several side-effects that may affect the empirical study of the triboelectric effect; these parasitic influences must be carefully considered and avoided. For example, Dickinson, Jensen, and Dion [45] found that at least in some cases, charging of the polymer samples was due only to slippage of the sample in the grips accompanied by charge transfer between the metallic grips and the polymer. Sometimes, the charge generation is accompanied by electrical discharges and optical emission [48], [49]. These phenomena and similar ones involving uncontrolled variables add to the difficulty of characterizing the triboelectric effects and may produce conflicting results.

This mainly empirical study first introduces several theoretical considerations on the anisotropy in Section 2; then it describes in Section 3 the experimental method, setups, and materials used. Section 4 presents a summary of the experimental results on the potential maps resulted from tribocharging; these potential maps are analyzed in Section 5 with several statistical means. Section 6 discusses the results and draws conclusions.

2. Anisotropy of the friction

There are several phenomena that may contribute to the anisotropy of the friction of polymeric materials, all depending on the technological manufacturing process. One is the production of macroscopic directional patterns on the surface of the material during manufacturing (Fig. 1), and is common in such processes as: (i) lamination (rolling) and thinning of plates; (ii) extrusion or cold drawing of bars and wires through a die. Other phenomena are microscopic, related to the material structure, such as packaging of the polymer chains during manufacturing; they are influenced by the thermal regime as well as the mechanical stress applied to the material, mainly during initial phases of fabrication. For some plastics and for specific technologies, such as those used in polyester and nylon (polyamide) fiber fabrication, the alignment of the fibers (by cold drawing) can reach almost perfect order, as in a crystal, with specific chemical bonds between the chains (hydrogen bonds form between the amide groups, thus modifying both the mechanical and electrical properties of the material). In anisotropically structured materials the friction coefficients may also depend on the direction of relative movement of the bodies in contact, especially when abrasion occurs. As a matter of fact, the fracture mechanisms depend on the elastic and plastic deformation coefficients, which – in such materials – differ according to the direction.

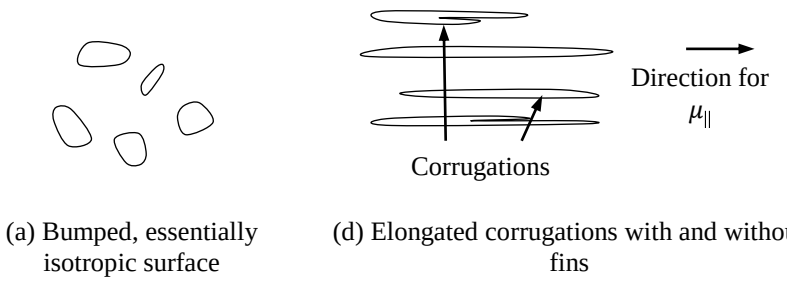

Fig. 1. Sketches of surface patterns that may explain isotropic and anisotropic, direction-dependent friction

The cumulative effect of the microscopic and macroscopic processes is that the friction coefficients (FC) are not the same along different directions. Conventionally, the movement direction with minimal value of the friction coefficient is named the preferred 'parallel' direction. In the case of a laminated surface, it corresponds to the direction of the striations. The respective friction coefficient is denoted by $\mu_{\parallel}$ (Fig. 1), and the one along the normal direction by $\mu_{\perp}$. There is no guarantee, however, that the maximal value of the friction coefficient is along the normal direction. Also, the friction forces along a specified direction

cannot be computed applying the two friction coefficients in a vectorial manner. When there is a prevailing direction in the patterned surface, usually named 'lay' that direction can be determined by visual inspection or by roughness profiling. The lay can be taken as preferred movement direction and denoted by the sign ||; along the lay, the sliding against a surface similarly or anisotropically patterned should be produced with minimal friction.

3. Experimental method and setup description

3.1. Measurement setups

The directionality (anisotropy) effect in the triboelectric charging of polymer slabs was studied using a custom-made setup composed of the electromechanical bench for sample tests, the electric potential measurement system, and the auxiliary devices for temperature mapping [5]. The electromechanical bench consists essentially in a reciprocating tribometry measurement bank that allows conformal-contact sliding movements with constant speed under friction forces that can be varied in a large range. The speed and the number of reciprocating movements are programmable. The system for measuring the potential on the tribocharged sample includes a computer-driven bidirectional *x-y* measuring table that carries the tribocharged sample and moves it under the electric potential measurement probe (Trek, model 3450). The potential values read by the electrostatic voltmeter (Trek, model P0865) are automatically recorded and stored. The basic experimental setup was described in [4] and [5], while details on the measuring method and several issues related to data processing were presented in [5], [50] - [53]. Details on the measurement conditions are given in subsections 3.3 and 3.4, including illustrations of the variation of the normal force, tangential force, and displacement, as measured by the sensors of the reciprocating tribometry equipment.

The roughness profiles of the slabs used in the experiments were also determined (using the device SurfTest Mitutoyo ver. 2.0; standard ISO 4287 – 1997, profile R, $\lambda_s = 2.5$ µm, cut-off at 0.8 mm, Gauss filter); in addition, the slabs were checked under microscopy under illumination with several colors for assessing the lay, as discussed in the next subsection.

3.2. Materials

The samples consisted of industrial grade slabs, cut from large sheets of PVC, ABS, and PS, taking precautions not to produce scratches on the surfaces to be tested. The materials under friction were, PVC for the lower sample, in all experiments, while ABS, for the upper sample. The PVC slabs had oriented corrugations, thus their surface presented geometric anisotropy. All slabs were electrically neutralized before each test using an air ionizer (model

ECA 88B, ELCOWA, Mulhouse, France), following the manufacturer's instructions. The material surfaces were inspected under optical microscope to determine the type of surface texturing and the lay. Pictures of typical surfaces of the samples are shown in Fig. 2. The PVC slab under white light exhibits a lay with the surface texturing characterized by long striations and with some smaller circular indentations. The PVC slabs photographed under yellowish light show, beyond the horizontal lay, pointwise surface defects (indentations).

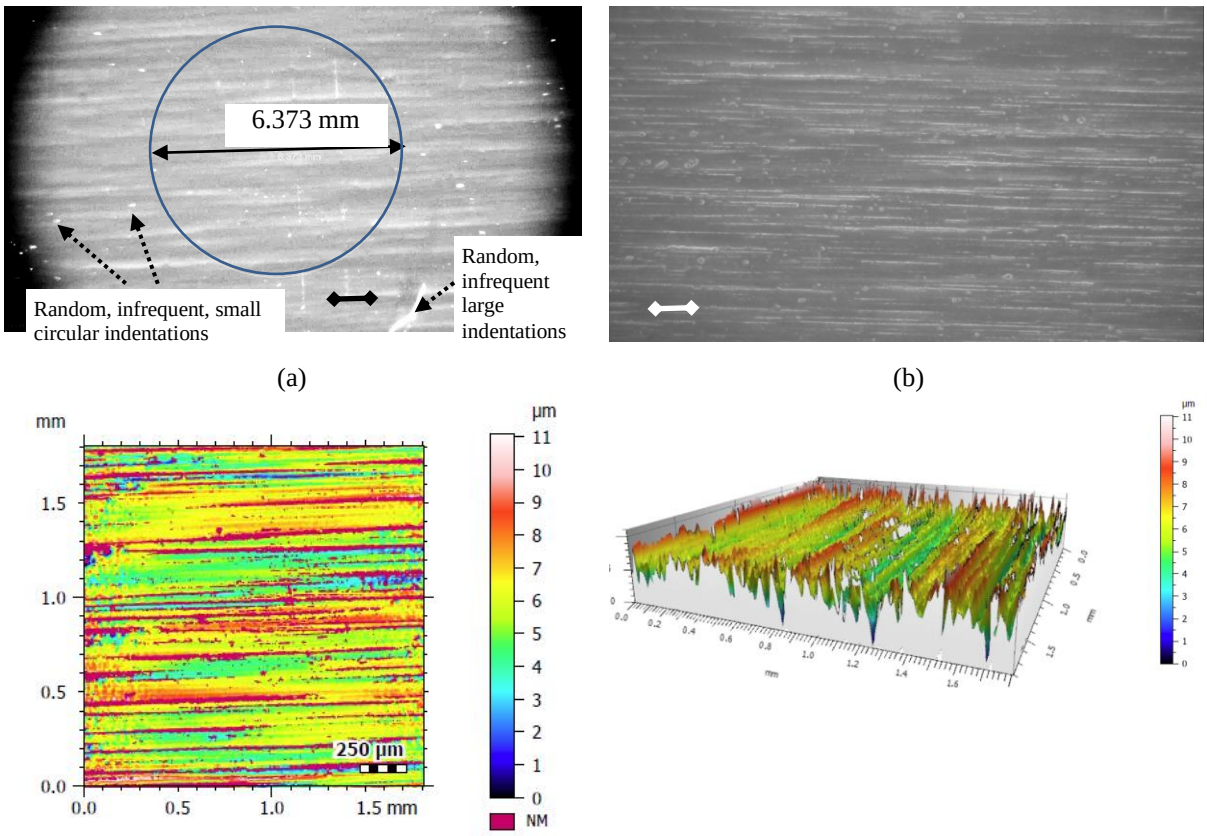

Fig. 2. Examples of surface texturing for the PVC slabs used in experiments. (a) Under yellow light, with small circular indentations better visible; (b) filiform striations are the main surface pattern (lay), well visible under white light. Pictures (a), (b) were processed for contrast and luminosity. Scale bars in Fig. 2(a) and 2(b) represent 1 mm. (c) and (d) Surface roughness profiles obtained before friction with the automated optical 3D profiler type Talysurf CCI 6000 (confocal interferometric roughness meter).

The PVC samples in Figs. 2 have surface textures with anisotropic features, with the lengths of the filiform striations (grooves) of the order of tens of millimeters while the transversal direction dimension is less than 0.2 mm, as it can be seen on the calibrated

pictures. Random indentations of the surface with average diameter of less than 0.50 mm and a few randomly oriented striations of about 0.1-5 mm in length are also present.

The ABS samples are textured but the texture is largely isotropic; some ABS samples present infrequent local anisotropic surface elements (grooves), which are visible under magnification, under suitable light direction and color (after contrast and luminosity modified for improved visibility of the texture in the pictures). Figure 3 shows examples of typical ABS surface patterns.

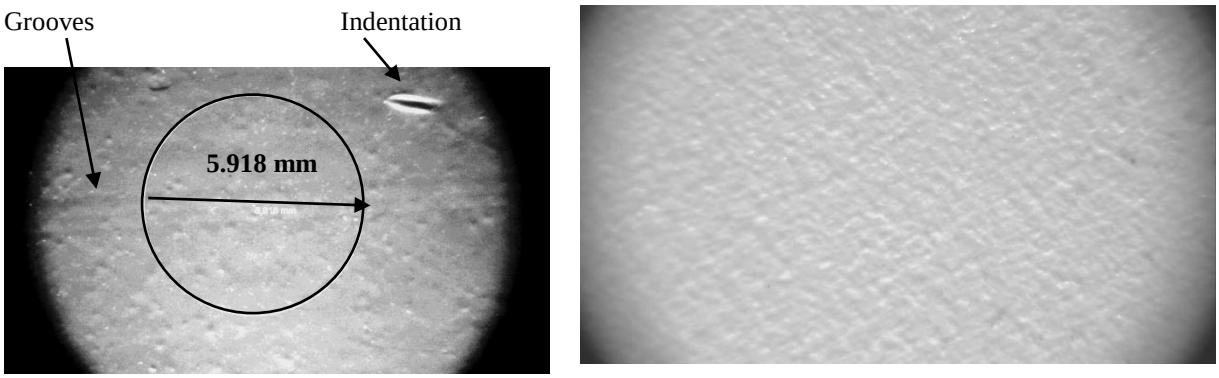

(a) (b)

Fig. 3. Examples of ABS surface patterning. While some linear defects appear on some samples under yellow light (a), the surface pattern is essentially isotropic with random distribution of small bumps and valleys (b).

The surfaces roughness profiles were determined along two orthogonal directions, one of them along the lay. An example of roughness profile for a PVC slab used in experiments is shown in Fig. 4 (sample 04A). All reported roughness measurements, average roughness *Ra*, root mean square roughness *Rq*, and mean roughness depth *Rz*, are based on ISO 4287-1997, profile R, $\lambda_s = 2.5$ µm, cut-off at 0.8 mm, and Gauss filter. For the sample in Fig. 4: $Ra = 0.075$ µm, $Rq = 0.095$ µm, $Rz = 0.463$ µm.

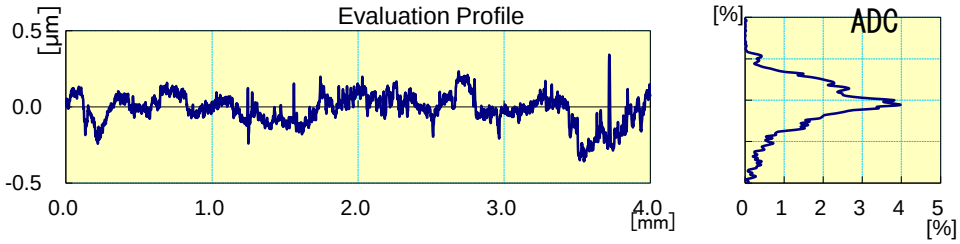

Fig. 4. Roughness linear profile and amplitude distribution curve, for a slab of PVC (04A), lay (||) direction.

The above data is for PVC in the parallel direction. An example of results obtained for the normal direction is given in Fig. 5, which shows the large amplitude and wide peaks and valleys (micro-waviness) due to the asperities of the material now appearing normal to the measuring direction (profile direction), with some periodicity. Notice the much wider and thicker tales of the amplitude distribution curve (ADC) in case of the normal profile. The values of Ra and Rz ($Ra = 0.755$ µm, $Rq = 0.921$ µm, $Rz = 4.146$ µm) are also strongly dissimilar to the ones for the parallel direction. These dissimilarities are robust indicators of the different friction coefficients in the two directions.

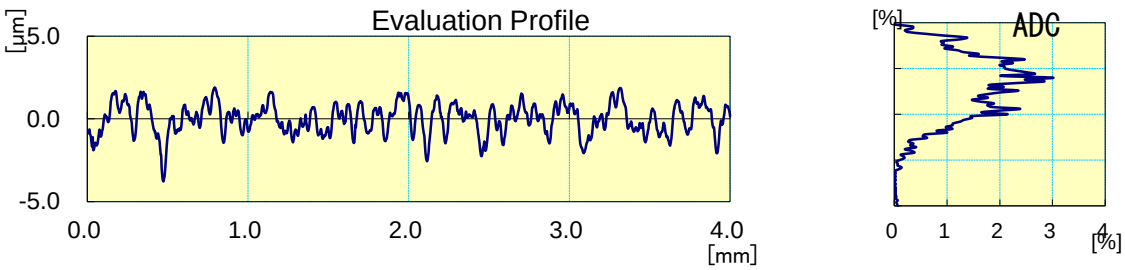

(a) (b)

Fig. 5. Roughness linear profile (a) and amplitude distribution curve (b), for the same slab of PVC (904A), normal (⊥) to the lay direction.

The ABS samples have an isotropic surface pattern, with almost circular 'bumps' and 'valleys' with virtually homogeneous distribution. Some scratches may have occurred by minor accidents in the manipulation previously of entering the laboratory. An example of typical roughness profile for the ABS slabs used in experiments is shown in Fig. 6. While some bumps have heights comparable with those of the striations on PVC slabs, the bumps are irregularly placed. Compared with the roughness profile of PVC ||, the ADC has a much larger range (wide 'bumps'). The roughness measurements produce $Ra = 0.219$ µm, $Rq = 0.290$ µm, $Rz = 1.441$ µm. The roughness parameters determined for ABS are given in the Table 1.

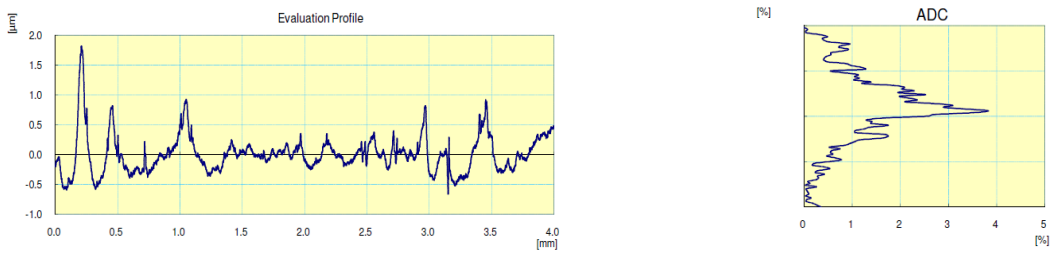

(a) (b)

Fig. 6. ABS linear roughness profile (a) and ADC (b); corresponding to the microscopic image in Fig. 3.

Table 1. Example of 2D roughness values for ABS slabs

ABS slabs	*Ra* µm	*Rq* µm	*Rz* µm
Parallel direction			
ABS 01	0.2190	0.2900	1.4410
ABS 02	0.1920	0.2490	1.3690
ABS 03	0.1560	0.2010	0.9020
AVERAGE	**0.1890**	**0.2467**	**1.2373**
STDV	**0.0316**	**0.0445**	**0.2926**
Normal direction			
ABS 901	0.4170	0.5180	2.1330
ABS 902	0.2580	0.3320	1.7780
ABS 903	0.2010	0.2680	1.7780
AVERAGE	**0.2920**	**0.3727**	**1.8963**
STDV	**0.1119**	**0.1299**	**0.2050**

Notice the great difference between the ABS roughness values and those for PVC, moreover the great difference between the PVC roughness measured along the lay direction and along the normal to the lay. The roughness parameters for the PVC slabs are given in the Table 2 and indicate a strong (about $\times 6$) difference in the *Ra* parameter between the roughness profiles along the lay direction and normal to it. The roughness values *Rq* obtained by the automated optical 3D profiler are comparable to the ones obtained by unidirectional tests with the device SurfTest Mitutoyo ver. 2.0. (The maximal values *Ra* and *Rz* cannot be compared because of the different statistics produced by the 2D and 3D measurements.)

Table 2. 2D roughness parameters for PVC slabs (values in µm)

Direction	parallel direction			normal direction		
Roughness parameter	*Ra*	*Rq*	*Rz*	*Ra*	*Rq*	*Rz*
PVC_01A	0.129	0.184	1.496	0.941	1.153	5.119
PVC_01B	0.105	0.13	0.659	0.812	0.979	4.08
PVC_02A, long PVC nr2	0.102	0.134	0.663	0.805	0.985	4.218
PVC_02B, square PVC nr2	0.146	0.186	1.15	0.864	1.067	4.712
PVC_03A	0.14	0.197	1.119	0.743	0.914	3.964
PVC_03B	0.16	0.198	1.084	0.746	0.925	4.237
PVC_04A	0.075	0.095	0.463	0.755	0.921	4.146
PVC_04AA+4A on another position	0.114	0.146	0.718	-	-	-
PVC_04B	0.224	0.274	1.213	-	-	-
PVC_05A	0.122	0.148	0.795	0.956	1.207	5.337
PVC_05B	0.188	0.24	1.209	0.751	0.948	4.305
PVC **averages**	**0.137**	**0.176**	**0.961**	**0.819**	**1.011**	**4.458**
PVC **STDV**	**0.042**	**0.052**	**0.316**	**0.083**	**0.107**	**0.486**

Using only the samples for which data was collected for both directions, the *t*-test (for different variances) produces *t Stat* =22.97, *t Critical two-tail* = 2.200, $P(T \leq t)$ *two-tail* = 1.2E-10, showing that the roughness values are statistically different in the two directions.

In addition to the tests described above, the surface profile was determined before and after wearing due to friction using the automated optical 3D profiler type Talysurf CCI 6000 (confocal interferometric roughness meter). For these 3D profiles, the settings were: magnification× 10, optical resolution 1.8 μm, maximum slope of the measured surface 7.7^{o}, measured area 1.8×1.8 mm.

3.3. Tests for tribocharging

All tests were performed under constant rubbing speed of 15 mm/s [52], which was found to create a high-enough level of charging. The distance of rubbing (stroke) was 50 mm, imposed by the setup. The upper (pressing) slab was kept fixed, while the movement of the bottom slab was alternative along the stroke, with 10 cycles of back and forth movement. The lower slab shape was always square (50×50 mm) for it can be removed and turned into the normal direction for repeating the test. Between tests, the slabs where discharged using an air ionizer (model ECA 88B, ELCOWA, Mulhouse, France), following the manufacturer's instructions. The upper slab had a contact (friction) surface of 10×10 mm². Throughout the paper, slabs are denoted by the first digit "0" when the friction force direction was parallel to the lay (surface orientation) under test, and by the first digits "90" when the orientation was normal.

The main electric quantity measured was the potential $V_{h,k}$ at 25 points, $h, k = 1, \ldots, 5$, with the position denoted by the number of the line ($h = 1 \ldots 5$), and the number of the column ($k = 1, \ldots, 5$) counting from the left. The columns are parallel and along the direction of friction during periodical back and forth motion. Ten cycles of rubbing, under a normal force of 10 N (nominal), were applied before measuring the potential. The potential was measured immediately after the friction cycles as described in [5]. The movement direction with respect to the measuring points on the sample is shown in Fig. 7. The measuring conditions were $RH = 40 - 45\%$ and $\theta = 25 - 27$ °C ambient temperature.

	C1	C2	C3	C4	C5
L1	1	6	11	16	21
L2	2	7	12	17	22
L3	3	8	13	18	23
L4	4	9	14	19	24
L5	5	10	15	20	25

Back and forth movement directions

Fig. 7. Measurement points at the surface of the bottom sample; the higher potentials tend to occur in the nine points of the central part.

3.4. Measured quantities during friction experiments

A detailed study of the setup used in the measurements, of the forces occurring during the process, and of the applied signal analysis was presented in [53]. The measured quantities included the tangential force $F_t(t)$ applied to the moving sample holder, the normal force $F_n(t)$ applied to the samples, the time variable displacement $d(t)$ of the moving sample holder, the electrical potential and the temperature map of the bottom sample immediately after the friction. Examples of temporal variations of $F_t(t)$, $F_n(t)$, and $d(t)$ are shown in Fig. 8.

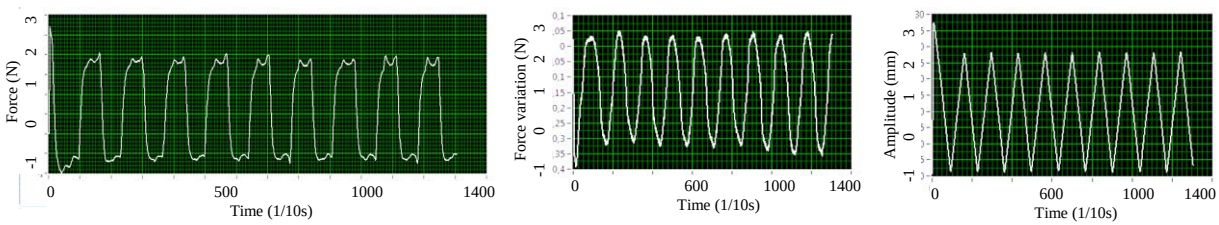

(a) Tangential force $F_t(t)$ (b) Normal force variation $\Delta F_n(t)$ (c) Displacement $d(t)$

Fig. 8. Examples of time variation of the measured quantities (friction between PVC and ABS samples)

The normal force applied to all samples was 10 N. The normal force variation, created by the vibrations produced during the movement, including vibrations due to the sliding of the samples, was recorded (Fig. 8 b) and taken into account in the computation of the work of the friction forces [53]. Notice that the variation of the normal force is less than 0.4 N (4%). As the reciprocating movement of the mechanisms used in the experiments has virtually no stops, the measurements are not affected by any stick-slip effect.

4. Experimental results

4.1. Potential measurement results

An example of the potential values measured for parallel and normal directions of sliding for PVC samples against ABS, is given in Table 3, and additional values in the Annex, Table A1. The highest values were consistently found toward the center of the slabs, irrespective of the orientation. Notice that some measured values at the borders of the slabs are anomalous, with reversed polarity. This might be explained by the interplay of three mechanisms. Because of the thermal dissipation, the center of the slab becomes hotter (see Fig. 9),a phenomenon that favors the accumulation of more charge in that area; the higher charge, in turn, repels same sign charges at the boundary of the slab; hence the charge reversal at the boundary. The strip of higher temperature occurring in Fig. 9 corresponds to an indentation of the sample due to stronger wearing, with significant abrasion. An example of non-uniform potential map is shown in Fig. 10.

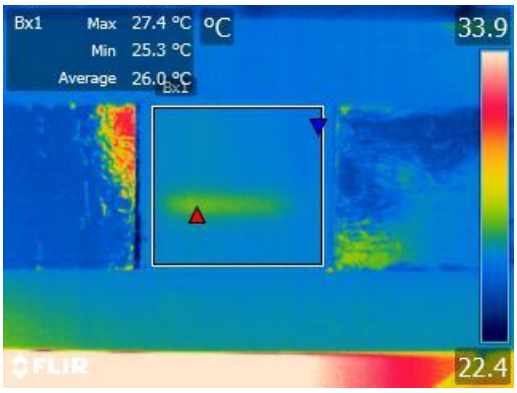

Fig. 9. Example of temperature map indicating non-uniform temperature (non-uniform heat generation), which partly correlates with the electric potential maps

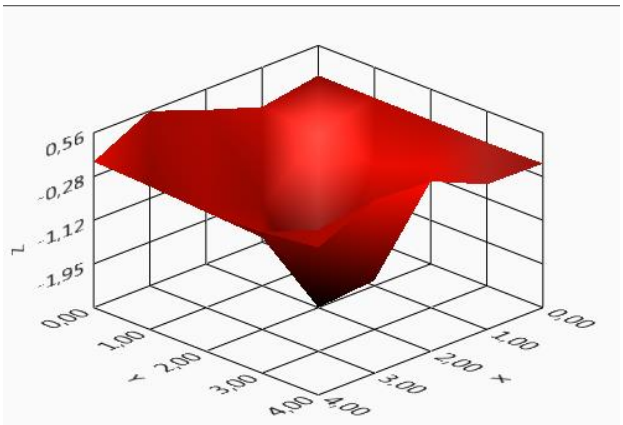

Fig. 10. Example of non-uniform electric potential map.

Table 3. Electric potential, $U_{\perp}, U_{||}$, measured for parallel and normal frictional sliding conformal contact, PVC vs. ABS corresponding to the slabs in Tables 1 and 2.

Sample Code 01A					Sample Code 901A				
-23.5	-91.1	-57.3	-43.5	-9.4	-28.7	-77.5	-92.6	-133.1	2.4
-48	-825.4	-657.7	-54.9	-3.8	-142.2	-1200.8	-1577.1	-319	-5.6
-30.4	-550	-526.9	-31.9	2.1	-743.3	-1083.9	-1646.6	-298.3	0.2
-9.6	-472	-522.4	-40	0.1	-90.8	-358.8	-1571.9	-120.6	-16.1
45.8	253.4	-781.4	-140.6	-9.9	76.1	835.5	489.5	-88.8	-16.8
Sample Code 02A					Sample Code 902A				
3.8	-17.6	-11.1	11.4	-1.4	-20.9	-59.5	-19.5	-10.1	-5.9
4	-733.9	-195.9	8.3	0.6	-74.5	-995.4	-1846.5	-72.3	-8.7
13.6	-748.1	-362.2	-14.4	3.6	-98.1	-938.9	-2258	-95.5	-6.6
8.4	-461.1	-346.3	-9.3	-0.4	-16	-329.4	-1458	-63.7	-0.2
17.5	370.7	158.9	0.6	-9	60	863.8	612.5	26.9	10.4
Sample Code 03A					Sample Code 903A				
-22	-25.9	-99.4	-15.7	-6	3.3	73.3	-101.4	-127.9	2.5
-68.6	-1242	-2194.8	-94.7	-13.4	-53.6	-967.7	-2824.2	-186.9	4.9
-44.9	-915	-3395	-148.1	-19.7	-65.3	-1146.5	-3735.7	-242.4	5.9
14.9	-468.7	-2010.9	-83.3	-16.1	-13.7	-616.7	-3035.9	-121.4	2.8
107.1	787.4	785.3	63.5	-10	85.1	1420.5	877	35.7	3.3

The averages of the potential differences between the two cases with different directions of movement are given in Table 4, along with the averages for the central values on the sample (central region as indicated in Fig. 7). The inter-samples charging variability is greater for parallel sliding, which produces lower charging, than for orthogonal sliding.

Table 4. The average values of the electric potential for the overall measuring points and the central ones, for samples 01, 02, and 03, respectively 901, 902, and 903.

Sample	Parallel, full (all points)	Parallel, central points	Normal, full	Normal, central	Difference normal-parallel, full (absolute value)	Difference normal-parallel, central (absolute value)
01	-185.1	-322.8	-328.3	-706.7	143.2	383.9
02	-92.372	-240.0	-272.1	-678.9	179.73	438.9
03	-365.44	-891.1	-429	-1086.1	63.56	195

The longitudinal (along the movement direction) and the transversal profiles of the electric potential are exemplified in Fig. 11. The variations of the potential are consistent with previous studies [50].

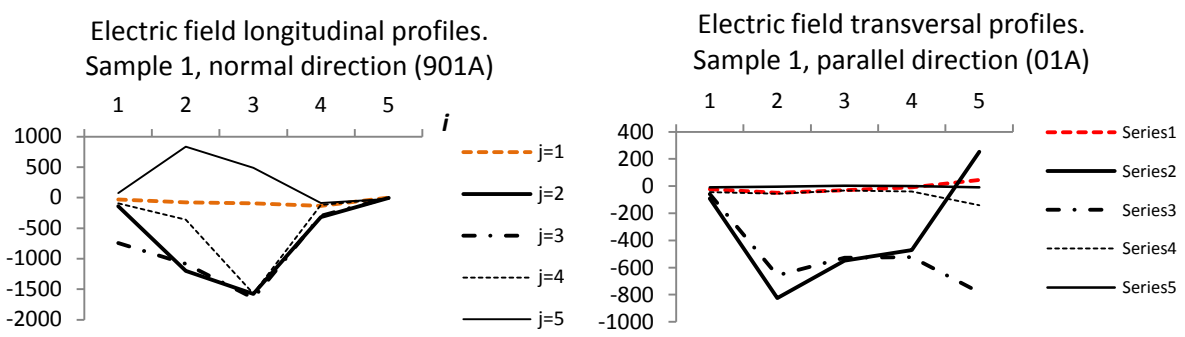

Fig. 11. Examples of longitudinal (left) and transversal (right) profiles of the electric potential, for the five ($j = 1, \dots, 5$) measurement lines, denoted by C1-C5 in Fig. 7.

The differences of the potentials created by parallel and orthogonal friction for three samples, given in Tables A2 and A3 in the Annex, also indicate a strong dependence of the tribocharging on the direction of movement.

4.2. Correlation of the electric potential maps for the parallel and normal directions

The repeatability of the tribocharging results for different PVC samples was verified using the correlation coefficients for the potentials. All Pearson cross-correlations were computed using the standard formula

$$C\left(U_*^h, U_*^j\right) = \frac{\sum_{k=1}^{n}\left(U_*^h(k) - \overline{U_*^h}\right) \cdot \left(U_*^j(k) - \overline{U_*^j}\right)}{\sqrt{\sum_{k=1}^{n}\left(U_*^h(k) - \overline{U_*^h}\right)^2} \cdot \sqrt{\sum_{k=1}^{n}\left(U_*^j(k) - \overline{U_*^j}\right)^2}},$$

where $\overline{U_*^h}$ and $\overline{U_*^j}$ are the averages, * stands for either $\perp$ or $||$, and k is the index of the current point, $n = 25$. For example, with these notations, $C(U_{||}^h, U_{||}^j)$, where h, j are two samples, is the correlation coefficients for parallel sliding, also briefly denoted by $C_{U_{||}, U_{||}}$.

The correlation coefficients for parallel sliding, $C_{U||,U||}$, were larger than 0.6 but lower than 0.72. For orthogonal friction, these coefficients, $C_{U\perp,U\perp}$, were all higher than 0.93, see Table 5. Because at the borders of the samples the values of the potential are more random, a better indication can be given by the averages computed on the central part of the slabs.

The correlations between the electric potential distributions for the parallel and normal directions, for samples (i,j), $i \neq j$, $i,j = 1,2,3$, are given in Table 5, which shows that the potential maps were almost perfectly correlated for the orthogonal friction direction (which has higher friction and potential), while for the parallel direction the correlations were weaker. Even stronger correlations were obtained for the central points for the differences of the potentials defined as $\Delta U_k = U_{\perp \mathrm{k}} - U_{||k}$, see Table 6.

Table 5. Correlation of the charging (electric potentials) for the parallel and normal directions, for the samples (i,j), $i \neq j$, $i,j = 1,2,3$

Correlations for the parallel direction		**Correlations for the orthogonal direction**	
corr(01,02), $C_{U||,U||}(1,2)$	0.717	corr(901,902)$C_{U\perp,U\perp}(1,2)$	0.958
corr(01,03), $C_{U||,U||}(1,3)$	0.602	corr(901,903)$C_{U\perp,U\perp}(1,3)$	0.935
corr(02,03), $C_{U||,U||}(2,3)$	0.657	corr(902,903)$C_{U\perp,U\perp}(2,3)$	0.982

Table. 6. Correlation of the potential maps for couples of slabs submitted to the same type of friction process, for the central points

corr (Diff 01,02)	0.826
corr (Diff 02,03)	0.733
corr (Diff 01,03)	0.688

The strong correlations between the triboelectric potential maps of different PVC samples after friction with the same ABS sample also show that the results are not random, but due to well-identified causes and repeatable processes. These results also show the triboelectric charging can be confidently used in industrial applications, such as energy harvesting, where repeatability is paramount.

4.3. Statistical analysis of the experimental results -Anisotropy verification

The statistics of the differences of the potentials on samples with friction parallel, respectively orthogonal to the surface pattern confirm the hypothesis of anisotropic tribocharging. The differences in electric potential are given in Table A3. The distribution of the differences is not strongly asymmetric with respect with 0 (Fig. 12); therefore, a simple

visual inspection is not enough convincing. Notice that the distribution in Fig. 12 is not Gaussian, therefore the p-value cannot be computed as for normal distributions.

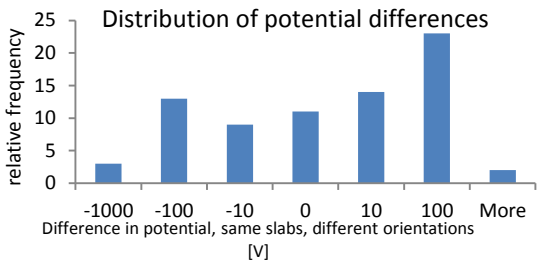

Fig. 12. Example of distribution of potential differences for PVC slabs after friction against ABS.

Applying the t-test to the differences between the electric potentials for the normal and parallel friction, as in the Table 8 lead to a convincing rejection of the hypothesis that the two directions of friction produce the same effect (null differences on average), with a p-value equal to 0.00063 << 0.05 for $n-1$ freedom degrees, where n is the number of values, and left tail. Considering a single degree of freedom, the p-value is 0.092 > 0.05. To further verify the hypothesis, the test was performed for the values in the central parts of the samples. When the differences are calculated only for the central columns, for $n-1$ freedom degrees, the p-value for the hypothesis of isotropic friction becomes of the order 10^{-20}. Using a single degree of freedom, the p-value is 0.014 < 0.05, clearly proving the hypothesis of anisotropic charging.

The demonstration of the statistical difference for the full potential maps of the tribocharged PVC samples is given in Table 9. For all pairs of tests, carried by sliding along the parallel and the normal directions, the differences of the potential maps are statistically true with high probability.

Table 9 demonstrates with confidence between 0.97 and 0.998 the distinction between the pair of potential maps obtained by triboelectric charging in the two normal directions. Tables 8 and 9 show that the direction of higher roughness of the surface of the samples was always associated with higher average squared values of the potential.

Table. 8. Set of values in the electric potential maps used to test the hypotheses of different statistics for the triboelectrification during sliding along the parallel and normal directions

	Sample 01A	Sample 901A	Sample 02A	Sample 902A	Sample 03A	Sample 903A	Sample 04A	Sample 904A	Sample 05A	Sample 905A
L1	23.5	28.7	3.8	20.9	22	3.3	-12.4	-27.8	-19.1	6.1
	48	142.2	4	74.5	68.6	53.6	-12.4	-7.8	-23	-3
	30.4	743.3	13.6	98.1	44.9	65.3	-12.1	6	-27.5	13.1
	9.6	90.8	8.4	16	14.9	13.7	-11.6	8.3	-29.3	-16.6
	45.8	76.1	17.5	60	107.1	85.1	-11.9	-6.8	-24.6	-71
L2	91.1	77.5	17.6	59.5	25.9	73.3	14	-154.1	202	-780.7
	825.4	1200.8	733.9	995.4	1242	967.7	13.9	-120.3	193.7	-518.6
	550	1083.9	748.1	938.9	915	1146.5	15.6	-57.6	21.2	-451.2
	472	358.8	461.1	329.4	468.7	616.7	16.3	-62.8	211.5	-613.7
	253.4	835.5	370.7	863.8	787.4	1420.5	10.1	-90.1	239	-788.6
L3	57.3	92.6	11.1	19.5	99.4	101.4	-2.7	-154.1	187.4	20.4
	657.7	1577.1	195.9	1846.5	2194.8	2824.2	-0.1	-120.3	-3.6	-20.8
	526.9	1646.6	362.2	2258	3395	3735.7	0.5	-57.6	-69.4	-12.7
	522.4	1571.9	346.3	1458	2010.9	3035.9	2.3	-62.8	-111.4	-23.2
	781.4	489.5	158.9	612.5	785.3	877	4.2	-90.1	-178.5	-103.3
L4	43.5	133.1	11.4	10.1	15.7	127.9	-5.8	-21.6	-33.6	0.6
	54.9	319	8.3	72.3	94.7	186.9	-5.8	-8.8	-56.2	0.7
	31.9	298.3	14.4	95.5	148.1	242.4	-6.2	-5.8	-63.2	-1.6
	40	120.6	9.3	63.7	83.3	121.4	-6.7	-5.4	-48.1	-7.9
	140.6	88.8	0.6	26.9	63.5	35.7	-7.6	-7.8	-73.1	-15.4
L5	9.4	2.4	1.4	5.9	6	2.5	-5	-2.4	-30	0
	3.8	5.6	0.6	8.7	13.4	4.9	-5	-0.3	-46.3	-0.3
	2.1	0.2	3.6	6.6	19.7	5.9	-5	0	-47.7	-0.2
	0.1	16.1	0.4	0.2	16.1	2.8	-4.9	-1.4	-44.2	1.1
	9.9	16.8	9	10.4	10	3.3	-4.9	-2.4	-37.5	2

Table 9. Student *t*-tests: Paired two PVC samples for averages (hypothesized mean difference is null; 25 observations, degrees of freedom *df* = 24)

	01A	*901A*	*02A*	*902A*	*03A*	*903A*	*04A*	*904A*	*05A*	*905A*
Mean	209.24	440.65	140.48	398.05	506.10	630.14	-1.73	-42.15	3.54	-135.39
Variance	75622.3	305497.1	52968.91	409075.0	745510.7	1116490.0	84.07	2685.14	12177.7	68346.86
Pearson Correlation	0.786		0.650		0.980		-0.694		-0.787	
t Stat	-3.070		-2.475		-2.281		3.452		1.957	
p(*T*<=*t*) one-tail	0.003		0.010		0.016		0.001		0.031	
t Critical one-tail	1.711									
p(*T*<=*t*) two-tail	**0.005**		**0.021**		**0.032**		**0.002**		**0.062**	
t Critical two-tail	2.064									

4.4. Relationship between charging and the roughness parameters

The relationship between the electric field and the roughness parameters was studied using a global variable for the field, namely the sum of squares of the measured potential values. The reason for using the square of the potential is to eliminate the sign. The variable was computed summing over all points of the samples (denoted by index A) and over the central columns C2, C3, C4 only (denoted by index C). The formal definitions are

$$S^2_{U^2,A} = \sum_{C1}^{C5} \sum_{i=1}^{5} U^2_{C_k,i}\,, \qquad S^2_{U^2,C} = \sum_{C2}^{C4} \sum_{i=1}^{5} U^2_{C_k,i}.$$

The squared values of the above, $S_{U^2,A}$ and $S_{U^2,C}$, were used to determine if there is a relationship between this indicator of the charging and the roughness parameters R_a, R_q, and R_z. It was found that there are linear regressions between $S_{U^2,A}$ and $S_{U^2,C}$, on one side, and R_a, R_q, and R_z, on the other side, for the parallel direction of friction (see Fig. A1 in the Annex). The linear regression equations are

$$S_{U\|^2,A} = 54680R_a - 4501.6, \qquad R^2 = 0.537,$$

$$S_{U\|^2,A} = 37837R_q - 4026.1, \qquad R^2 = 0.649,$$

$$S_{U\|^2,A} = 2485.2R_z - 544.59, \qquad R^2 = 0.279.$$

The equations for $S_{U^2,C}$ are very similar, as the columns C1 and C5 have lower values of potential. Interestingly, the regression lines for the normal friction direction are virtually insignificant, with coefficients of determination less than $R^2 = 0.123$ and with negative slopes. For example, for R_z, the regression is $S_{U\|^2,A} = -1243.7R_z + 8657.2$, $R^2 = 0.123$. These results show that different tribocharged generation processes occur at higher friction coefficients as found for the normal direction of friction and for large normal forces (10 N) as used in the experiments. The stronger abrasion observed for the normal direction friction might explain why the roughness indices are no more directly related to the potential values obtained by tribocharging.

The strong differences in the linear regressions equations, including the respective coefficients of determinations, are reinforcing the conclusion that direction-dependence is an important aspect of tribocharging.

5. Discussion and conclusions

The main hypothesis of this study was proved: A highly anisotropic triboelectric charging effect is produced in samples of PVC slabs having surfaces with directional patterns during back and forth movements in frictional conformal contact with ABS slabs, even if the latter have isotropically patterned surfaces.

The anisotropy of the triboelectric effect was found to be mainly due to the anisotropy of the friction (i.e., unequal friction coefficients along orthogonal directions, $\mu_{\perp} \neq \mu_{\parallel}$ due to anisotropically patterned surfaces). This purely-empirical qualitative explanation refers to the macroscopic level. A quantitative analysis of the anisotropy of the triboelectric charging effect can be done at microscopic level by taking into account the roughness indices that characterize the surfaces in contact.

During the tests, wearing of the surfaces was noted. However, it has not modified the main pattern of the surfaces, as shown by the 3D profiles displayed in Fig. 13 (before friction) and Fig. 14 (after friction) and the roughness parameters given in Table 10. The reduced wearing is explained by the similar values of the hardness of the surfaces; Vickers hardness of PVC and ABS, as determined for the slabs used in the experiments, all were roughly in the same interval (9 to 10 HV).

The correlations of the charging maps between different pairs of slabs indicate that the triboelectric charging can be confidently used in industrial applications, where repeatability is paramount. Better repeatability of the results can be obtained for friction in the normal direction. This observation has implications in the use of the triboelectric effect in sensors. It also suggests a solution for improving the design of the electrodes (i.e., the region of triboelectric power collection) for triboelectric generators. However, the effect needs to be further investigated.

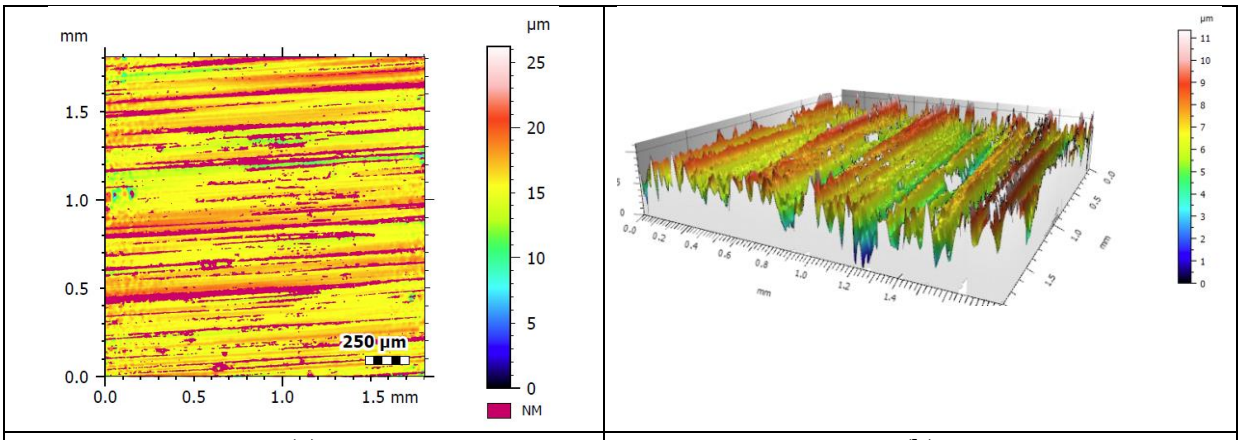

(a) (b)

Fig. 13. Example of 3D profile of a PVC sample, before friction.

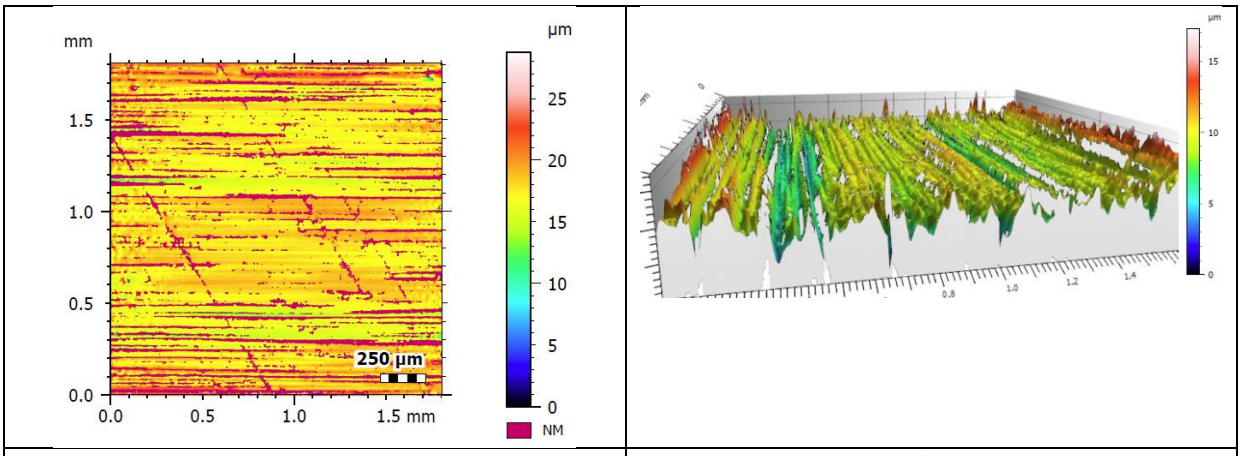

(a) (b)

Fig. 14. The 3D profile of the same PVC sample after the friction test, with moderate wearing.

Table. 10. Surface roughness parameters before and after friction (ISO 25178)

Parameter	Before [μm]	After [μm]
Sa	1.12	1.165
Sq	1.450	1.528
Sz	11.338	17.273

The anisotropy has implications on applications where the charging needs to be kept consistent with the friction force, such as in sensors, and in applications where the efficiency of the charge generation needs to be optimized. Reducing the charging induced by friction is important in electronics manufacturing, as well as in chemical, petro-chemical, and textiles industries. For uses in energy harvesters based on tribocharging, the materials and the friction forces should be chosen so that wearing does not change the initial lay of the surfaces.

Further work should be done to study the anisotropy of the triboelectric charging of polymers under friction with different normal forces.

Acknowledgments

All the experiments were performed in IUT Angouleme, University of Poitiers, France, using the equipment of “Tribo-electrostatics” research team of PPRIME Institute, UPR 3346 CNRS – University of Poitiers- ENSMA. The setup used for data acquisition was made by several current and former members of this team; the version of the setup used in this study is due to Dr. B. Neagoe, Y.E.P. TZ and L.D, with some feedback from HNT. The authors are much indebted to Mr. Omar Tilmatine for help with the surface scanning measurements.The very helpful comments made by the Editor and the referees are acknowledged with thanks.

Conflict of Interest: The authors declare no competing financial interest.

Authors' contribution. HNT proposed the study, processed most of the data, and wrote a preliminary version of the paper. YEP and HNT performed the tribocharging experiments with help from LD, while TZ performed the surface hardness and rugosity measurements. All authors discussed and interpreted the results and agreed with the final form of the paper.

References

[1] Gajewski JB, Gatner K. Interpretation of the results of research on tribocharging in a rotating shaft-oil-lip seal system. J Electrostat 2009;67:365–371. doi:10.1016/j.elstat.2008.12.015.

[2] Gajewski JB, GŁogowski MJ, Gatner K, Gawliński M. ZDDP content in mineral and synthetic motor base oils and its effect on electrostatic and tribological phenomena in a rotating shaft-oil-lip seal system. Tribol Int 2010;43:1012–6. doi:10.1016/j.triboint.2009.12.061.

[3] Alahmadi A. Influence of triboelectrification on friction coefficient. Int J Sci Eng Res 2014;5:22–9.

[4] Neagoe B, Prawatya Y, Zeghloul T, Souchet D, Dascalescu L. Laboratory bench for the characterization of triboelectric properties of polymers. J Phys Conf Ser 2015;646. doi:10.1088/1742-6596/646/1/012058.

[5] Neagoe B, Teodorescu HN, Prawatya Y, Dascalescu L, Zeghloul T. Experimental bench for studying the relation between the dynamic characteristics of the frictional motion and the electric potential at the surface of polymer slabs in sliding conformal contact. Tribol Int 2017;111:107–15. doi:10.1016/j.triboint.2017.03.006.

[6] Li J, Wu G, Xu Z. Tribo-charging properties of waste plastic granules in process of tribo-electrostatic separation, Waste Manag; 2015; 35: 36-41.

[7] Iuga A, Samuila A, Morar R, Bilici M, Dascalescu L. Tribocharging techniques for the electrostatic separation of granular plastics from waste electric and electronic equipment. Part Sci Technol; 2016; 34: 45–54.

[8] Mekhalef-Benhafssa A, Messal S, Medles K, Zeghloul T, Dascalescu L. Factors that influence the efficiency of a propeller-type tribocharging device for granular plastics, IEEE Trans Ind Appl; 2017; 53:1446-1451.

[9] Younes K, Younes M, Meziane R, Samuila A, Dascalescu L. Modified tribo-charging device for the electrostatic separation of plastics from granular industrial wastes. Separ Sci Technol; 2017; 52: 1246 - 1256.

[10] Lungu M. Electrical separation of plastic materials using the triboelectric effect. Min Eng; 2004; 17: 69–75.

[11] Dascalescu L, Zeghloul T, Iuga A. Electrostatic separation of metals and plastics from waste electrical and electronic equipment. In WEEE Recycling. Research, Development,

and Policies (Chagnes A, Cote G, Ekberg E, Nilsson M, Retegan T, Eds), Elsevier, Amsterdam, 2016, pp. 53-74.

[12] Zhu G, Chen J, Liu Y, Bai P, Zhou YS, Jing Q, et al. Linear-grating triboelectric generator based on sliding electrification. Nano Lett 2013;13:2282–9. doi:10.1021/nl4008985

[13] Bai P, Zhu G, Liu Y, Chen J, Jing Q, Yang W, et al. Cylindrical rotating triboelectric nanogenerator. ACS Nano 2013;7:6361–6. doi:10.1021/nn402491y.

[14] Niu S, Liu Y, Wang S, Lin L, Zhou YS, Hu Y, et al. Theory of sliding-mode triboelectric nanogenerators. Adv Mater 2013;25:6184–93. doi:10.1002/adma.201302808.

[15] Tang W, Meng B, Zhang HX. Investigation of power generation based on stacked triboelectric nanogenerator. Nano Energy 2013;2:1164–71. doi:10.1016/j.nanoen. 2013. 04.009.

[16] Bai P, Zhu G, Zhou YS, Wang S, Ma J, Zhang G, Wang ZL. Dipole-moment-induced effect on contact electrification for triboelectric nanogenerators. Nano Res; 2014; 7: 990–997.

[17] Niu S, Zhou YS, Wang S, Liu Y, Lin L, Bando Y, et al. Simulation method for optimizing the performance of an integrated triboelectric nanogenerator energy harvesting system. Nano Energy 2014;8:150–6. doi:10.1016/j.nanoen.2014.05.018.

[18] Teklu AA, Sullivan RM. A prototype DC triboelectric generator for harvesting energy from natural environment 2017;86;34-40.

[19] Yun BK, Kim JW, Kim HS, Jung KW, Yi Y, Jeong MS, Ko JH, Jung JH. Base-treated polydimethylsiloxane surfaces as enhanced triboelectric nanogenerators Nano Energy; 2015;15:523–529.

[20] Lim N, Hong D, Kim C, Jeong J, Kwon KH. Inductively coupled plasma surface modification of polyethylene terephthalate and application in a triboelectric generator. Thin Solod Films; 2017;637:27-31.

[21] Hu Y, Yang J, Jing Q, Niu S, Wu W, Wang ZL. Triboelectric nanogenerator built on suspended 3d spiral structure as vibration and positioning sensor and wave energy harvester. ACS Nano 2013;7:10424–32. doi:10.1021/nn405209u.

[22] Yi Y, Lin L, Niu S, Yang J, Wu W, Wang S, Liao Q, Zhang Y, Wang ZL Self-powered trajectory, velocity, and acceleration tracking of a moving object/body using a triboelectric sensor. Advanced Functional Materials 2014;24:7488-7494.

[23] Su Y, Zhu G, Yang W, Yang J, Chen J, Jing Q, Wu Z, Jiang Y, Wang ZL. Triboelectric sensor for self-powered tracking of object motion inside tubing. ACS Nano; 2014; 8: 3843-3850.

[24] Garcia C, Trendafilova I, de Villoria RG, del Rio JS. Self-powered pressure sensor based on the triboelectric effect and its analysis using dynamic mechanical analysis. Nano Energy 2018;50:401-409.

[25] Liu W, Zhang C, Lin H, Qu W, Wang X. Texture and sliding motion sensation with a triboelectric nanogenerator transducer. Sensors and Actuators A: Physical 2017;256:89-94.

[26] Zhang B, Huang W, Wang J, Wang X. Comparison of the effects of surface texture on the surfaces of steel and UHMWPE. Tribol Int 2013;65:138–45. doi:10.1016/j.triboint.2013.01.004.

[27] Kim D, Jeon SB, Kim JY, Seol ML, Kim SO, Choi YK. High-performance nanopattern triboelectric generator by block copolymer lithography. Nano Energy 2015;12:331–8. doi:10.1016/j.nanoen.2015.01.008.

[28] Menezes PL, Kailas SV. Role of surface texture and roughness parameters on friction and transfer film formation when UHMWPE sliding against steel. Biosurface and Biotribology 2016;2:1–10. doi:10.1016/j.bsbt.2016.02.001.

[29] Lu P, Wood RJK, Gee MG, Wang L, Pfleging W. The use of anisotropic texturing for control of directional friction. Tribol Int 2017;113:169–81. doi:10.1016/j.triboint.2017.02.005.

[30] Andersson S, Söderberg A, Björklund S. Friction models for sliding dry, boundary and mixed lubricated contacts. Tribol Int 2007;40:580–7. doi:10.1016/j.triboint.2005.11.014.

[31] Vladescu SC, Medina S, Olver A V., Pegg IG, Reddyhoff T. Lubricant film thickness and friction force measurements in a laser surface textured reciprocating line contact simulating the piston ring-liner pairing. Tribol Int 2016;98:317–29. doi:10.1016/j.triboint.2016.02.026.

[32] Lu P, Wood R, Gee M, Wang L, Pfleging W. The friction reducing effect of square-shaped surface textures under lubricated line-contacts—an experimental study. Lubricants 2016;4:26. doi:10.3390/lubricants4030026.

[33] Lu P, Wood R, Gee M, Wang L, Pfleging W. The use of microscopic texturing for control of directional friction. Tribol Int 2017;113:169-181. doi:10.1016/ j.triboint.2017.02.005.

[34] Gao Z, Fu W, Wang W, Kang W, Liu Y. The study of anisotropic rough surfaces contact considering lateral contact and interaction between asperities. Tribol Int 2018;126:270-282.

[35] Henniker J. Triboelectricity in polymers. Nature 1962;196:474. doi:10.1038/196474a0.

[36] Pham R, Virnelson RC, Sankaran RM, Lacks DL. Contact charging between surfaces of identical insulating materials in asymmetric geometries. J Elstat 2011;69:456-460.

[37] Shinohara I, Yamamoto F, Anzai H, Endo S. Chemical structure and electrostatic properties of polymers. J Electrostat 1976;2:99–110. doi:10.1016/0304-3886(76)90001-2.

[38] Williams MW. Triboelectric charging of insulating polymers-some new perspectives. AIP Adv 2012;2. doi:10.1063/1.3687233.

[39] Watson PK. The transport and trapping of electrons in polymers. IEEE Trans Dielectr Electr Insul 1995;2:915–24. doi:10.1109/94.469986.

[40] Diaz AF, Felix-Navarro RM. A semi-quantitative tribo-electric series for polymeric materials: The influence of chemical structure and properties. J Electrostat 2004;62:277–90. doi:10.1016/j.elstat.2004.05.005.

[41] Burgo TAL, Ducati TRD, Francisco KR, Clinckspoor KJ, Galembeck F, Galembeck SE. Triboelectricity: Macroscopic charge patterns formed by self-arraying ions on polymer surfaces. Langmuir 2012;28:7407–16. doi:10.1021/la301228j.

[42] Dickinson JT, Jensen LC, Park MK. Time correlations of electron and positive ion emission accompanying and following fracture of a filled elastomer. Appl Phys Lett 1982;41:443–5. doi:10.1063/1.93544.

[43] Dickinson JT, Jensen LC. Fracto-emission from filled and unfilled polybutadiene. J Polym Sci Polym Phys Ed 1985;23:873–88. doi:10.1002/pol.1985.180230504.

[44] Dickinson JT, Jensen LC, Langford SC, Dion RP, Nick L. Molecular CO emission accompanying fracture of polycarbonate: evidence for chain cleavage. J Mater Res 1993;8:14–7. doi:10.1557/JMR.1993.0014.

[45] Dickinson JT, Jensen LC, Dion RP. Fracto-emission from high density polyethylene: Bond breaking versus tribological stimulation. J Appl Phys 1993;73:3047–54. doi:10.1063/1.352987.

[46] Hoy EP, Mazziotti DA, Seideman T. Development and application of a 2-electron reduced density matrix approach to electron transport via molecular junctions. J Chem Phys 2017;147. doi:10.1063/1.4986804.

[47] Henry PSH. The role of asymmetric rubbing in the generation of static electricity. Br J Appl Phys 1953;4. doi:10.1088/0508-3443/4/S2/313.

[48] Teodorescu HN, Irimia M, Sofron E, Simionescu C. The optical emission stress analysis method. Theory and applications. In: VDI-Verlag, editor. Exp. Mech. Forsch. und Prax. 10. GESA-Symposium, Augsburg: VDI-Verl; 1987, p. 287–96.

[49] Teodorescu HN, Sofron E, Cr S, Popa M. Unconventional techniques for jointing testing under stress in microelectronics. In: Kraft W, editor. Join. Ceram. Glas. Met., Bad Nauheim: DGM-Informationsges.-Verl.; 1989, p. 333–6.

[50] Neagoe MB, Prawatya YE, Zeghloul T, Dascalescu L. Electric-potential-measurement-based methodology for estimation of electric charge density at the surface of tribocharged insulating slabs. J Electrostat 2017;90:123–30. doi:10.1016/j.elstat.2017.10.007.

[51] Prawatya Y, Senouci K, Zeghloul T, Neagoe B, Dascalescu L, Medles K. Statistical process control of the tribocharging of polymer slabs in frictional sliding contact. 2017 IEEE Ind Appl Soc Annu Meet IAS 2017;2017–January:1–6. doi:10.1109/IAS.2017.8101698.

[52] Prawatya YE, Neagoe MB, Zeghloul T, Dascalescu L. Optimization of continuous triboelectrification process for polymeric materials in dry contact. IOP Conf Ser Mater Sci Eng 2017;174. doi:10.1088/1757-899X/174/1/012067.

[53] Teodorescu HN, Yopa Prawatya, Thami Zeghloul LD. Signal processing and error reduction for reciprocating triboelectrometry. Proc Rom Acad Ser A-Mathematics Phys Tech Sci Inf Sci 2018;19:509–18.

[54] Deltombe R., Kubiak K.J., Bigerelle M, How to select the most relevant 3D roughness parameters of a surface (2011), Scanning. doi: 10.1002/sca.21113, which

has been published in final form at http://onlinelibrary.wiley.com/doi/10.1002/sca.21113/abstract

Annex 1

Table A1. Potential maps measured for PVC vs. ABS slabs

06MAPING					07MAPING					08MAPING				
c1	c2	c3	c4	c5	c1	c2	c3	c4	c5	c1	c2	c3	c4	c5
-0.0004	-0.2983	0.0988	-0.0008	-0.0010	-0.0361	-0.6750	-0.0218	0.0378	-0.0115	-0.0203	-0.5919	0.1050	0.1479	-0.0071
-0.0042	-0.8359	-1.5412	-0.0613	0.0094	-0.0509	-0.1483	-1.4501	-0.1528	-0.0364	-0.0247	-0.2120	-1.0054	-0.0797	-0.0020
-0.0105	-0.7924	-0.9933	-0.1027	0.0189	-0.0013	-0.0800	-1.0487	-0.1515	-0.0084	0.0023	-0.1644	-1.1754	-0.0946	0.0085
-0.0178	-0.7526	-0.8908	-0.0036	0.0190	-0.0529	-0.5524	-1.0317	-0.1052	-0.0397	0.0178	-0.5024	-1.8102	-0.0825	0.0500
-0.0397	0.0151	0.1852	-0.0032	0.0000	-0.0521	-0.0297	0.2618	-0.0176	-0.0386	0.0229	0.0161	-0.8331	0.0052	0.1376

906MAPING					907MAPING					908MAPING_				
c1	c2	c3	c4	c5	c1	c2	c3	c4	c5	c1	c2	c3	c4	c5
-0.0112	-0.6868	0.1355	0.1982	-0.0016	0.0006	0.0730	1.4528	0.0209	0.0070	0.0034	-0.6429	0.0535	0.5253	0.0103
-0.0014	-0.8872	-2.1056	-0.0225	-0.0316	-0.0033	-1.0218	-2.1864	-0.3713	0.0007	0.0389	-0.5099	-3.1917	0.0596	-0.0007
-0.0348	-0.6476	-1.7054	-0.1361	-0.0022	-0.0243	-0.2593	-1.5151	-0.2797	-0.0196	-0.0299	-0.4056	-2.7668	-0.1533	-0.0127
-0.0478	-0.7090	-1.2646	-0.0645	0.0164	-0.0771	-0.0725	-3.0210	-0.1145	-0.0287	-0.0501	0.9036	-1.4670	-0.1870	0.0086
-0.0302	-0.0208	0.2598	0.0794	0.0942	-0.0246	0.0512	0.1709	0.1357	-0.0055	-0.0392	0.0038	1.3608	0.0197	0.0260

Table A2. Evidencing of the triboelectrification differences between the parallel and normal sliding directions for PVC vs. ABS using the method of the sum of squared potential values (roughly, proportional with the energy of the electric fields)

	06MAPING	07MAPING	08MAPING	906MAPING	907MAPING	908MAPING
C1	-0.00041	-0.03606	-0.0203	-0.01117	0.000603	0.003375
	-0.00422	-0.05089	-0.02468	-0.00143	-0.00331	0.038852
	-0.01048	-0.00125	0.002338	-0.03481	-0.02426	-0.02988
	-0.01777	-0.05289	0.017828	-0.04781	-0.07714	-0.05006
	-0.03973	-0.05206	0.0229	-0.0302	-0.02463	-0.03917
C2	-0.29828	-0.67499	-0.59189	-0.68679	0.073007	-0.64287
	-0.83587	-0.14827	-0.21202	-0.88723	-1.02181	-0.50987
	-0.79237	-0.07998	-0.16439	-0.64759	-0.25928	-0.40559
	-0.7526	-0.55238	-0.50238	-0.70901	-0.07253	0.903587
	0.015087	-0.02967	0.016144	-0.02081	0.051235	0.003791
C3	0.098772	-0.02176	0.104997	0.135548	1.45275	0.053522
	-1.54118	-1.45006	-1.00544	-2.10559	-2.18642	-3.19173
	-0.99332	-1.04872	-1.17542	-1.70544	-1.51511	-2.76675
	-0.89082	-1.03171	-1.81024	-1.26455	-3.021	-1.46702
	0.185219	0.261768	-0.83306	0.25977	0.170863	1.360847
C4	-0.00083	0.03779	0.147885	0.198249	0.020944	0.525284
	-0.06132	-0.15282	-0.07971	-0.02253	-0.37131	0.059628
	-0.10268	-0.15146	-0.09461	-0.13606	-0.27965	-0.15331

	-0.00364	-0.10521	-0.08248	-0.06452	-0.11447	-0.187
	-0.00322	-0.01758	0.005176	0.079442	0.13568	0.01975
C5	-0.00102	-0.01149	-0.00714	-0.00163	0.00698	0.01026
	0.009369	-0.03643	-0.00196	-0.03155	0.00069	-0.0007
	0.018902	-0.00842	0.008471	-0.00222	-0.0196	-0.0127
	0.018965	-0.03966	0.050021	0.016382	-0.0286	0.00863
	0	-0.03864	0.137608	0.094216	-0.0055	0.02597
SUMSQ for all columns C1-C5	6.198839	5.19899	7.116893	11.29179	19.7231	23.849
SUMSQ only for C2-C4	6.196011	5.184995	7.09346	11.2771	19.71468	23.84153

Notice in Table A2 that an indicator for the equivalent of the energy of the field (the sum of squared local potentials) is two to four times larger for the normal direction compared to the parallel direction (6.19 vs. 11.29, 5.19 vs. 19.72, and 7.11 vs. 23.8). Also notice that the central columns of the slabs carry almost all the electrical (tribocharging) energy, while the external points have a negligible contribution.

Table. A3. Differences of the potentials created by parallel and orthogonal friction, $U_{\perp} - U_{||}$, for three samples

Sample	**Differences** $U_{\perp} - U_{||}$				
01-901A	5.2	-13.6	35.3	89.6	-11.8
	94.2	375.4	919.4	264.1	1.8
	712.9	533.9	1119.7	266.4	1.9
	81.2	-113.2	1049.5	80.6	16.2
	-30.3	-582.1	-1270.9	-51.8	6.9
02-902A	24.7	41.9	8.4	21.5	4.5
	78.5	261.5	1650.6	80.6	9.3
	111.7	190.8	1895.8	81.1	10.2
	24.4	-131.7	1111.7	54.4	-0.2
	-42.5	-493.1	-453.6	-26.3	-19.4
03-903A	-25.3	-99.2	2	112.2	-8.5
	-15	-274.3	629.4	92.2	-18.3
	20.4	231.5	340.7	94.3	-25.6
	28.6	148	1025	38.1	-18.9
	22	-633.1	-91.7	27.8	-13.3

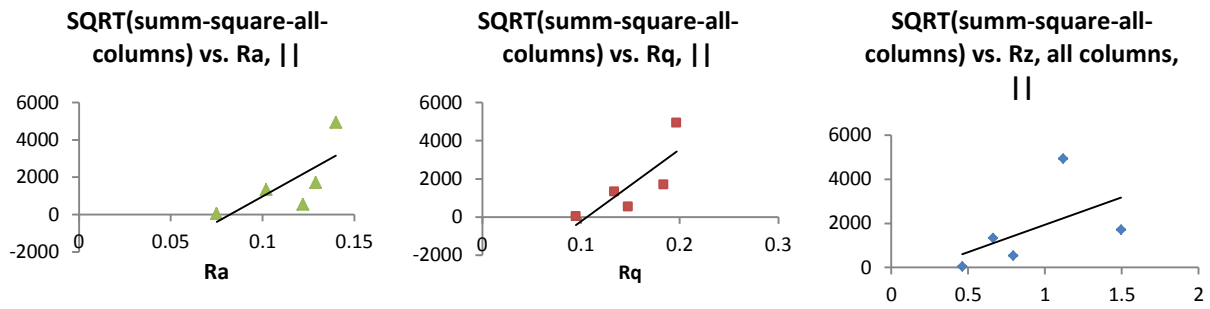

Fig. A1. Linear regressions for the square root of the sum of squares of the potentials versus the roughness indices.